SAND2014-19687J

Detection and modeling of leakage current in AlGaN-based UV LEDs

Michael W. Moseley, Andrew A. Allerman, Mary H. Crawford, Jonathan J. Wierer, Jr., Michael L. Smith, and Andrew M. Armstrong
Sandia National Laboratories, Albuquerque, New Mexico, USA, 87185

Abstract

Current-voltage (IV) characteristics of two AlGaN-based deep ultraviolet (DUV) light-emitting diodes (LEDs) with differing densities of open-core threading dislocations (nanopipes) are analyzed. A three-diode circuit is simulated to emulate the IV characteristics of the DUV-LEDs, but is only able to accurately model the lower leakage current, lower nanopipe density DUV-LED. It was found that current leakage through the nanopipes in these structures is rectifying, despite nanopipes being previously established as inherently n-type. Using defect-sensitive etching, the nanopipes are revealed to terminate within the p-type GaN capping layer of the DUV-LEDs. The circuit model is modified to account for another p-n junction between the n-type nanopipes and the p-type GaN, and an excellent fit to the IV characteristics of the leaky DUV-LED is achieved.

INTRODUCTION

Solid-state deep ultraviolet (DUV) light-emitting diodes (LEDs) and laser diodes (LDs) have a diverse set of potential applications in medicine,[1] public health,[2] and security.[3] These devices could also be used to enhance or enable other electronic technologies such as optical data storage[4] and photolithography.[5] The tunable bandgap of the $Al_xGa_{1-x}N$ materials system enables these alloys to be engineered and customized to fit a specific need,[6] such as DNA inactivation.[7] Despite the potential impact of high-efficiency DUV emitters and substantial efficiency gains in recent years,[8] AlGaN-based DUV-LEDs still have external quantum efficiencies that fall behind more developed InGaN-based visible light emitter technologies.[9]

High Al-content $Al_xGa_{1-x}N$ alloys are susceptible to the formation of threading dislocations and point defects as a result of the lower surface mobility of Al adatoms and the lack of a native lattice-matched substrate.[10] These defects can have many types of detrimental effects on optoelectronic devices, such as acting as non-radiative recombination centers[11] or electrical current leakage paths.[12] Although a great deal of effort has been invested into the suppression, mitigation, and annihilation of these crystalline defects,[13-15] further improvement is warranted to increase optoelectronic device external quantum efficiencies and enable widespread application of AlGaN-based DUV-LEDs.[16]

Open-core threading dislocations[17] have been shown to limit the performance of electronic and optoelectronic devices through electrical current leakage.[18-20] Also known as "nanopipes", these dislocations have been described as hollow tubes with (10-10) facets in the epitaxially grown material and have been observed to range in size from 2 nm to 50 nm.[21] Nanopipes can be detected through atomic force microscopy (AFM), conductive AFM (CAFM), transmission electron microscopy (TEM), and even optical microscopy with the assistance of defect-sensitive etching.[21-23] Recently, the mechanism of electrical current transport through these dislocations has been attributed to oxygen impurities segregated along the nanopipe inner wall.[24-26] Oxygen atoms contribute to Ga-O complexes which act as shallow donors and form a conductive impurity band approximately 78 meV below the conduction band, potentially shunting electric current and bypassing quantum wells or p-n junctions. In this way, nanopipes are particularly deleterious to optoelectronic device performance. However, the atomic-level mechanism of nanopipe formation is not yet clear,[27] which obscures the prevention of these defects during growth.

In this work, the electrical characteristics of open-core threading dislocations in $Al_{0.7}Ga_{0.3}N$ alloys and DUV-LEDs are investigated. Current-voltage (IV) characteristics of UV-LEDs with different nanopipe densities and IV characteristics of individual nanopipes in $Al_{0.7}Ga_{0.3}N$ are discussed. A three-diode circuit is constructed using SPICE [28] to model the electrical behavior of UV-LEDs with different nanopipe densities. Finally, a defect-sensitive etch is applied to high nanopipe density $Al_{0.7}Ga_{0.3}N$ and DUV-LEDs, confirming implications of the circuit model and yielding insight into nanopipe behavior in DUV-LEDs.

EXPERIMENTAL

Epitaxial heterostructures of $Al_{0.7}Ga_{0.3}N$/AlN and DUV-LEDs were grown in a Veeco D-125 metalorganic chemical vapor deposition (MOCVD) chamber at 75 Torr. Trimethylgallium (TMG), trimethylaluminum (TMA) and ammonia were used as precursors to grow the $Al_{0.7}Ga_{0.3}N$ layers, while silane and bis(cyclopentadienyl)magnesium were used as dopants. Substrates used for the growth of these films were (0001) c-plane sapphire misoriented 0.2° toward the m-plane.

The $Al_{0.7}Ga_{0.3}N$ templates consisted of 1.3 μm of Si-doped $Al_{0.7}Ga_{0.3}N$ with an electron concentration of 4×10^{18} cm^{-3} grown on a 3.75 μm AlN buffer layer on sapphire. All of the $Al_{0.7}Ga_{0.3}N$ templates had a total threading dislocation density of 3×10^{9} cm^{-2} determined by x-ray diffraction.[29] A defect-selective hot phosphoric acid etch was used to decorate and quantify open-core threading dislocations in the $Al_{0.7}Ga_{0.3}N$ templates.[21] A 150 nm thick Mg-doped GaN layer was grown on one template for electrical characterization by CAFM and defect-sensitive etching.

DUV-LED structures with a peak emission wavelength of 270nm were then grown on the n-$Al_{0.7}Ga_{0.3}N$ templates. The DUV-LED structure consisted of a 500 nm thick Si-doped n-$Al_{0.65}Ga_{0.35}N$ contact layer, a 3-period multi-quantum well (MQW) active region, a Mg-doped $Al_{0.9}Ga_{0.1}N$ electron blocking layer, and a 150 nm thick Mg-doped GaN p-contact layer. The active region consisted of $Al_{0.44}Ga_{0.56}N$ QWs and $Al_{0.55}Ga_{0.45}N$ barriers that were nominally 2.6 nm and 4.3 nm thick, respectively. The doping in the n-contact layer and the p-contact layer were 9×10^{18} electrons/cm^3 and 5×10^{17} holes/cm^3, respectively. The as-grown LED structures were then processed into fabricated into 300 μm × 300 μm devices.[30,31]

The current-voltage characteristics of the fabricated DUV-LEDs were modeled using the freely available LTspice program from Linear Technology Corporation.[28] Vertical current leakage paths through the Si-doped $Al_{0.7}Ga_{0.3}N$ templates and the p-type GaN / n-type $Al_{0.7}Ga_{0.3}N$ junctions were located and analyzed in air using a Bruker Nanoscope V scanning probe microscope with a CAFM attachment and Bruker RMN-12PT300B platinum probes. Details regarding the CAFM measurement and defect-sensitive etch can be found elsewhere.[32]

RESULTS AND DISCUSSION

Two DUV-LEDs with a similar total threading dislocation density of 3×10^9 cm^{-2} but different nanopipe densities were investigated. The nanopipe densities were determined using a defect-sensitive etch on $Al_{0.7}Ga_{0.3}N$ templates produced in the same growth run as the underlying $Al_{0.7}Ga_{0.3}N$ templates used for each DUV-LED. In a previous study, the distribution of etch pits was found to be similar across multiple $Al_{0.7}Ga_{0.3}N$ templates produced in the same growth run. Therefore, the nanopipe densities of the UV-LEDs can be accurately quantified without directly interfering with the growth surface of the underlying template. The average density of nanopipes in DUV-LED A was 1.1×10^4 cm^{-2}, which translates to approximately 10 nanopipes per 300 μm × 300 μm device. The average density of nanopipes in DUV-LED B was 1.2×10^6 cm^{-2}, which translates to approximately 1100 nanopipes per 300 μm × 300 μm device.

Shown in Figure 1 are current-voltage (IV) responses of both DUV-LEDs A and B, which have separate regimes marked by dashed lines. The electrical mechanisms that dominate each regime are: series resistance (0V-0.5V), carrier recombination in the space-charge region (0.5V-3.25V), carrier recombination in the quasi-neutral region (3.25V-7V), and shunt resistance (>7V).[33] However, DUV-LED B exhibited an effectively lower turn on voltage of 2V (versus 3.25V for DUV-LED A), and up to two orders of magnitude larger current between 2V and 4.5V of applied bias. This elevated level of current is attributed to the higher density of electrically conductive nanopipes in DUV-LED B.[19]

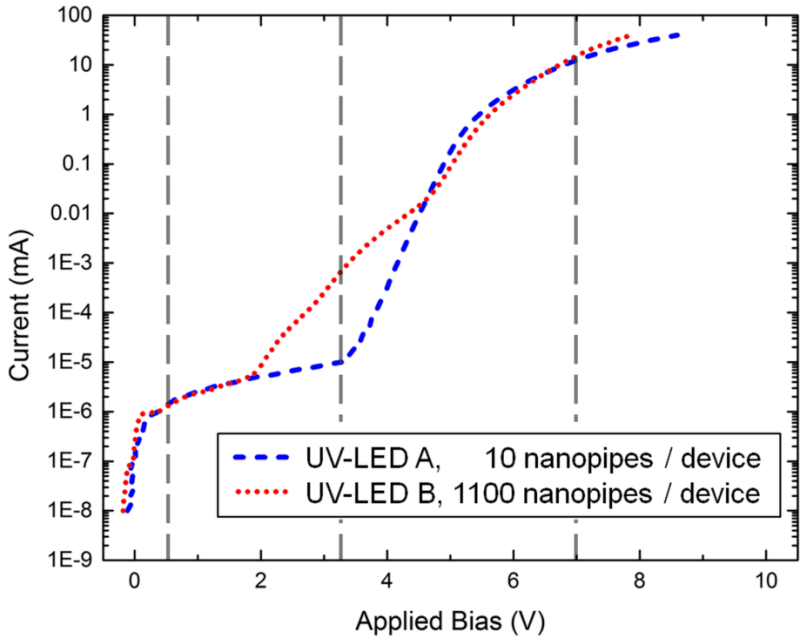

Figure 1. IV curves of two UV-LEDs with different open-core threading dislocation (nanopipe) densities. Both LEDs exhibit regimes dominated by shunt resistance, carrier recombination in the space charge region, carrier recombination in the quasi-neutral region, and series resistance.

The DUV-LEDs IV characteristics were modeled with LTspice[28] using the three-diode circuit shown in Figure 2. The three diodes in the circuit model represent carrier recombinations in the space-charge region of the diode, carrier recombinations in the quasi-neutral region of the diode, and a small Schottky barrier at the contact.[23] Parameters for each of the ideal diodes and resistors in the circuit were extracted from the DUV-LED IV responses in Figure 1. The IV characteristics of the simulated and fabricated DUV-LEDs are plotted together in Figure 3.

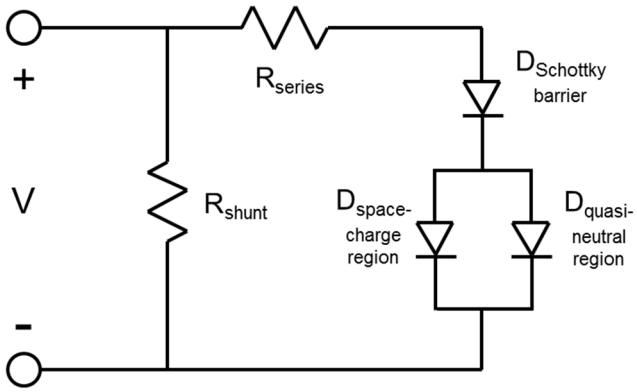

Figure 2: Equivalent circuit model, consisting of three diodes and two resistors, simulated in SPICE to emulate the IV characteristics of the DUV LEDs in this study.

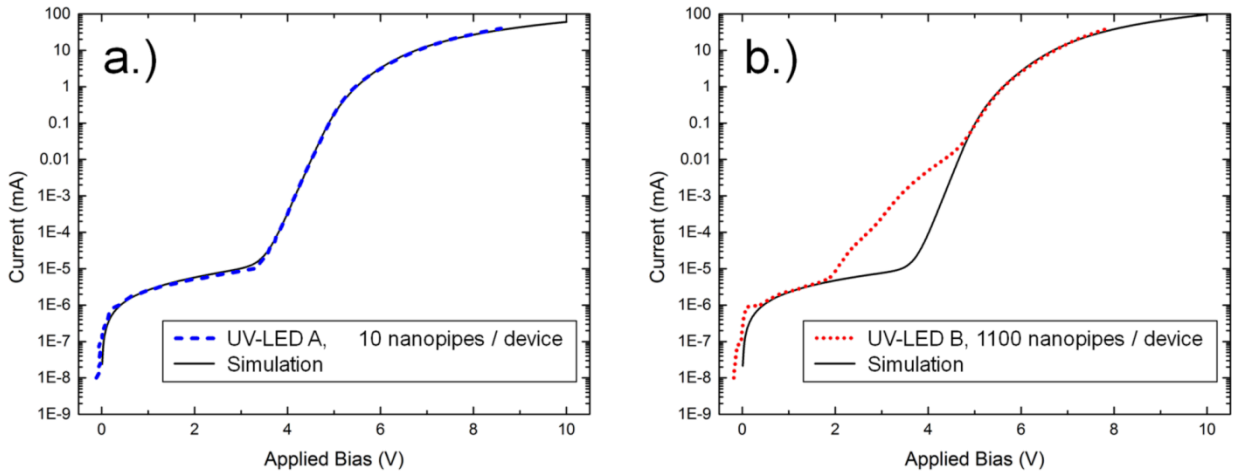

Figure 3. Current-voltage characteristics (dashed lines) of fabricated DUV-LEDs, and SPICE simulations (solid lines) of DUV-LED circuits using the three-diode model shown in Figure 2. An excellent fit was achieved between the measured and modeled IV of (a.) DUV-LED A with approximately 10 nanopipes, but an acceptable fit could not be established for (b.) the DUV-LED B with approximately 1100 nanopipes.

In Figure 3(a), there is a good agreement between the modeled and measured IV data for DUV-LED A, demonstrating that the three-diode circuit model in Figure 2 is capable of emulating low-leakage DUV-LED IV curves. However, an acceptable fit could not be established between the modeled and measured IV data for DUV-LED B as shown in Figure 3(b), which had a nanopipe density two orders of magnitude higher than that of DUV-LED A. The modeled IV characteristic of DUV-LED B deviates from the experimentally recorded IV data from 2V to 4.5V, and could not be reconciled by manipulating the parameters of the circuit elements shown in Figure 2. Thus, the circuit model in Figure 3 is unable to emulate high-leakage UV-LEDs, and must be modified to achieve a better fit to the measured IV characteristics.

As shown by the IV in Figure 3(b), the deviation between the measured and modeled IV characteristics is non-linear in nature. This behavior is somewhat counter-intuitive, since electrical conduction by nanopipes should be analogous to current through a resistor. The nonlinearity of the leakage current from 2 to 4.5V in the measured IV characteristic of DUV-LED B suggests that a more complex phenomenon is involved.

To electrically probe individual nanopipes in the epitaxially grown materials, CAFM was performed on the n-$Al_{0.7}Ga_{0.3}N$ templates and the p-GaN / n-$Al_{0.7}Ga_{0.3}N$ heterostructures. The p-GaN / n-$Al_{0.7}Ga_{0.3}N$ heterostructure consisted of the n-$Al_{0.7}Ga_{0.3}N$ template with a p-GaN cap layer, and is similar to a typical DUV-LED structure, only without the quantum wells and electron block layer. Conductive silver paste was applied to a diamond scribe mark on each sample to maintain electrical contact to the n-type layers, while the voltage of the platinum CAFM tip was varied between -10V to +10V. This measurement proved difficult since nanopipes are not only difficult to observe by optical microscopy, but also have been shown to rapidly passivate when electrically probed.[34] This characteristic inhibits the use of CAFM to find a nanopipe in an area before collecting a localized IV characteristic. Therefore, a brute force technique was employed, whereas the CAFM was periodically moved across the surface, and a separate IV characteristic was recorded at each micron in length across the path.

Most IV characteristics were predictably collected on non-leaking locations, where < 2nA of current was measured at an applied bias of 10V. In contrast, CAFM current at some locations exceeded 500 nA with an applied bias less than 7.5V. These discrete locations of increased CAFM current are attributed to a nanopipe in the material directly under the CAFM tip. Several IV characteristics recorded at nanopipe locations in an n-$Al_{0.7}Ga_{0.3}N$ template are shown in Figure 4(a), while the IV characteristics recorded at nanopipe locations in a p-GaN / n-$Al_{0.7}Ga_{0.3}N$ heterostructure are shown in Figure 4(b). The inset of Figure 4(b) also shows an IV characteristic of a non-leaking location on the p-GaN / n-$Al_{0.7}Ga_{0.3}N$ heterostructure, but on a much smaller current scale.

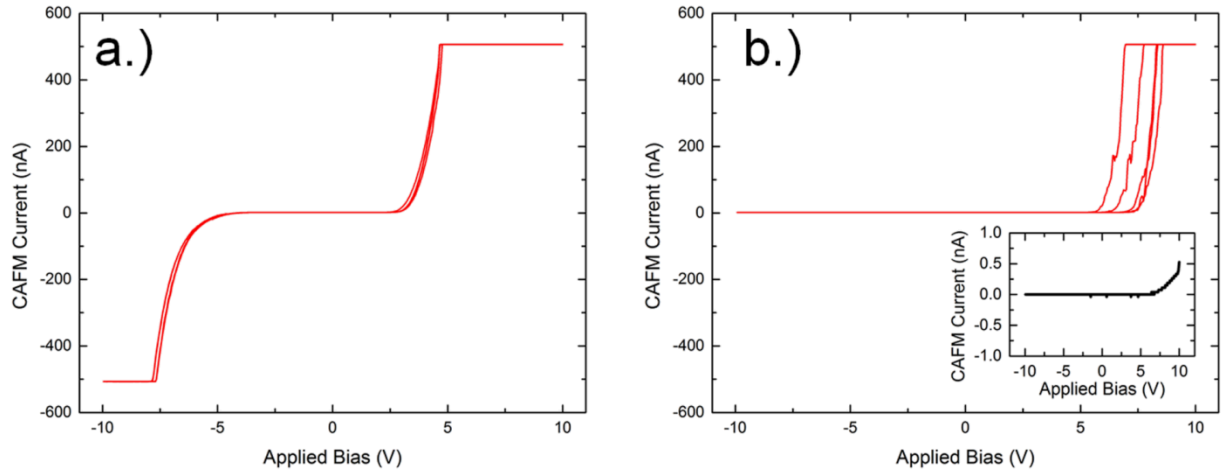

Figure 4: IV characteristics at electrical current leakage sites on (a.) an n-type $Al_{0.7}Ga_{0.3}N$ template exhibiting conduction in both forward- and reverse-bias, and (b.) a p-type GaN / n-type $Al_{0.7}Ga_{0.3}N$ junction exhibiting rectifying behavior. An IV characteristic of a non-leaking location of the p-type GaN / n-type $Al_{0.7}Ga_{0.3}N$ junction is shown in the (b.) inset.

As shown by the IV characteristics recorded at a nanopipe on the n-type $Al_{0.7}Ga_{0.3}N$ template in Figure 4(a), current is able to pass through the nanopipe in both forward and reverse bias. The ~5V required to turn on the leakage, in either forward or reverse bias, is the result of the relatively poor contact between the CAFM tip and the sample surface. In this case, the nanopipe behaves simply as a resistor.

On the contrary, as shown by the IV characteristic recorded at a nanopipe in the p-type GaN / n-type $Al_{0.7}Ga_{0.3}N$ heterostructure in Figure 4(b), current is only able to pass through a nanopipe in forward bias for the available voltage range. In this case, the formation of a p-n junction causes the nanopipe to behave like a diode. To confirm that the IV characteristic in Figure 4(b) is actually recorded at a nanopipe and is not the electrical response of the LED itself, another IV characteristic recorded at a non-leaking location in the p-n heterostructure, and is included as an inset of Figure 4(b). This inset is plotted on a drastically smaller current scale, illustrating that hardly any current is able to conduct in either forward or reverse bias for the applied voltage range. At maximum forward bias of +10V, the diode itself is just beginning to turn on as indicated by the slight increase in current. This information indicates that nanopipes are indeed the source of the non-linear, diode-like behavior of the leakage current in the high nanopipe density DUV-LED in Figure 3(b).

The diode-like behavior of the leakage in the p-GaN / n-$Al_{0.7}Ga_{0.3}N$ heterostructures suggests that the nanopipe terminates at (or within) the p-GaN without threading all the way to the device surface. The termination of the nanopipe at the p-GaN interface would be consistent with the non-linear behavior of the leakage sites. Since a nanopipe acts as a highly conductive n-type material, the adjacent p-GaN would form a different p-n junction with the nanopipe. An illustration of this hypothesized behavior of nanopipes in these UV-LED structures is shown in Figure 5.

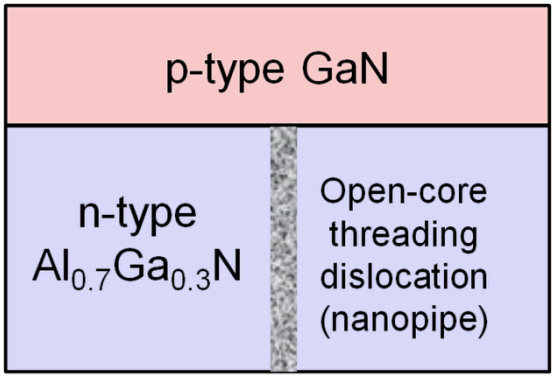

Figure 5: Illustration of a nanopipe threading path in the p-GaN / n-$Al_{0.7}Ga_{0.3}N$ heterostructure grown to elucidate the non-linear IV behavior exhibited by the high-leakage LED in Figure 3(b).

Defect-sensitive etching was used to test this hypothesis. This process consists of using phosphoric acid heated to 160 °C to enlarge nanopipes so they can be observed and quantified by an optical microscope.[22] This nanopipe decoration is accomplished by anisotropic etching along the (10-10) inner walls of the dislocation's open core. However, the acid is only able to enter these nanopipes and laterally etch if the dislocations thread to the surface of the epitaxially grown material.

To this end, this etch process was applied to an n-$Al_{0.7}Ga_{0.3}N$ template and a p-GaN / n-$Al_{0.7}Ga_{0.3}N$ heterostructure. Both samples are expected to have a similar distribution of nanopipes, since the n-$Al_{0.7}Ga_{0.3}N$ templates in each sample were produced in the same growth run. Before etching, microscope images of similar locations on both samples were recorded and are shown in Figure 6. After etching the same areas were revisited for further analysis. Microscope images of similar locations of both samples after etching are shown in Figure 7.

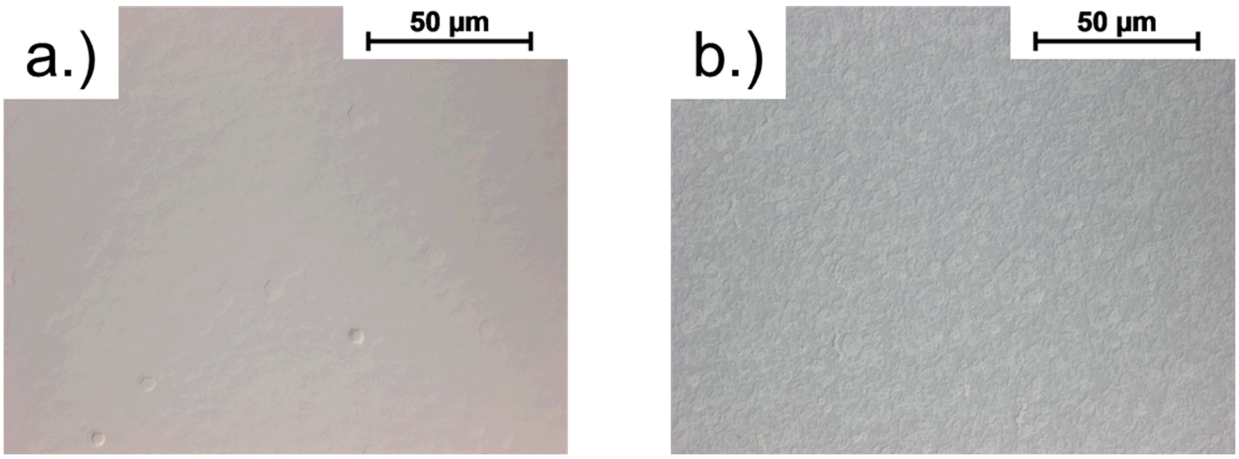

Figure 6: Optical microscope images at 50X magnification of (a.) an n-type AlGaN template and (b.) a p-type GaN / n-type $Al_{0.7}Ga_{0.3}N$ heterostructure. The n-type $Al_{0.7}Ga_{0.3}N$ layers in both (a.) and (b.) were produced in the same growth run.

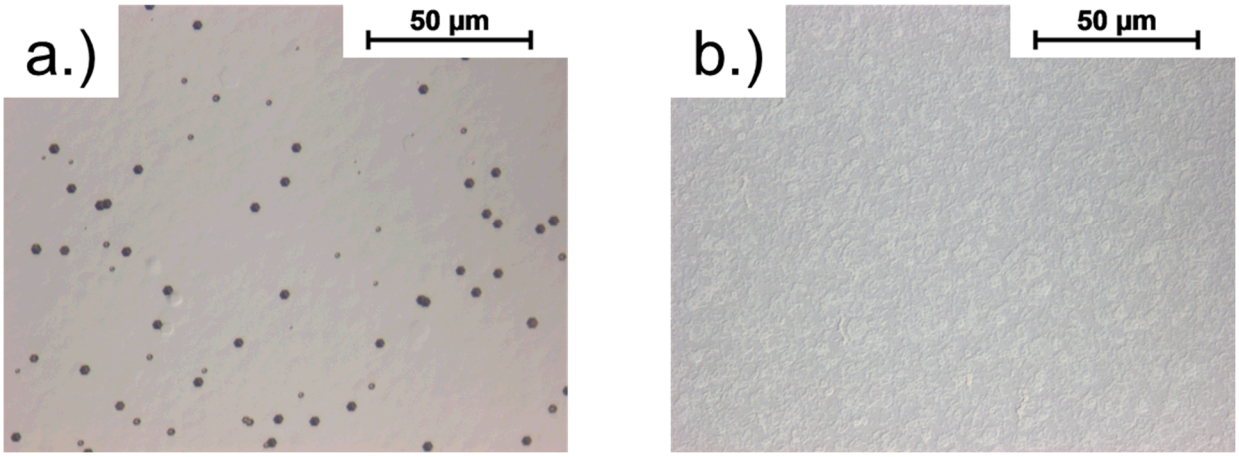

Figure 7: Optical microscope images at 50X magnification of (a.) an n-type AlGaN template and (b.) p-GaN / n-$Al_{0.7}Ga_{0.3}N$ heterostructure after being etched for 90 seconds in hot phosphoric acid. In (a.), open-core screw-type threading dislocations are decorated by micron-scale hexagonal pits, but in (b.) no etch pits are visible.

Before etching, neither sample showed visible signs of nanopipes, as shown in Figure 6. After etching, hexagonal etch pits are observed in the n-type AlGaN template, indicating the nanopipes thread to the surface of the material, as shown in Figure 7(a). Contrarily, no hexagonal pits are observed in the after-etch microscope image of the p-GaN / n-$Al_{0.7}Ga_{0.3}N$ heterostructure in Figure 7(b), indicating the nanopipes did not thread to the surface.

These data support the hypothesis that nanopipes are terminated either at the p-GaN / n-$Al_{0.7}Ga_{0.3}N$ interface or within the p-GaN layer. Therefore, p-n junctions would be formed at the nanopipe/p-GaN interfaces, resulting in rectifying leakage paths. It has been observed both in this study and previously in others that nanopipes easily thread through n-type and unintentionally-doped GaN.[35] However, Mg-doped GaN is resistant to the propagation of similar defects as a result of the surfactant effect of Mg.[36] It has been previously reported that Mg-doped GaN exhibits faster lateral coalescence[37] and the ability to overgrow V-defects.[38] Therefore, the termination of nanopipes within the p-GaN is attributed to the enhanced lateral growth afforded by the addition of Mg to the surface.

The circuit model shown in Figure 2 can be modified to reflect this new understanding of nanopipe propagation in DUV-LEDs. Shown in Figure 8 is the modified circuit model, which includes a diode and series resistor in parallel with the rest of the circuit to account for the effect of the p-n junctions between the nanopipes and the p-GaN capping layer. The DUV-LED with a high density of nanopipes, DUV-LED B, was modeled with LTspice now using the modified circuit model in Figure 8. The IV characteristic of the modeled leaky DUV-LED is plotted with the IV characteristic of the fabricated DUV-LED B in Figure 9. The resistance used for the nanopipe series resistor was 47 KΩ. As shown in Figure 9, there is a close fit between the modeled and measured IV data for DUV-LED B, demonstrating that the circuit model in Figure 8 is useful for emulating high nanopipe density DUV-LED IV curves, and that large densities of nanopipes can cause additional diode behavior in DUV-LEDs.

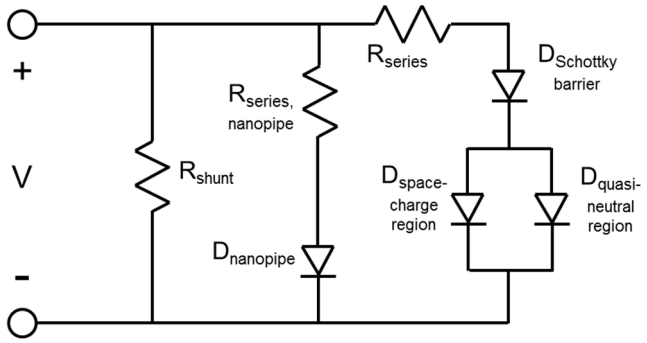

Figure 8: Modified circuit model with an additional diode and resistor in parallel with the rest of the circuit to emulate the non-linear behavior of the nanopipe leakage paths in DUV LEDs.

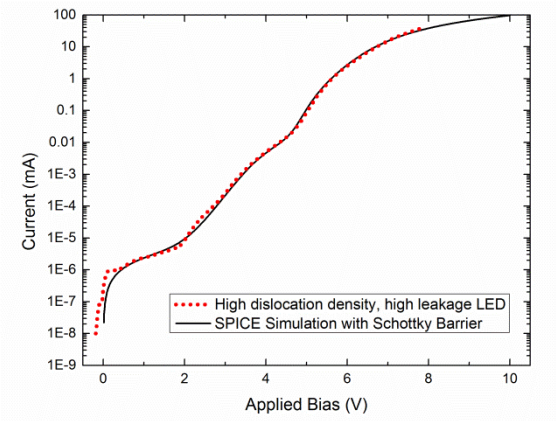

Figure 9: Current-voltage characteristics of fabricated DUV-LEDs (dashed lines), and SPICE simulations of DUV-LED circuits (solid lines) using the modified circuit model shown in Figure 8. After including the additional circuit elements, an excellent fit was achieved between the measured and modeled IV characteristics of DUV-LED B with approximately 1100 nanopipes.

CONCLUSION

In this study, two DUV-LEDs with nanopipe densities that differed by two orders of magnitude were grown and characterized. A simple three-diode circuit was used to model the IV characteristics of these DUV-LEDs in LTspice. While the circuit was able to accurately model the DUV-LED with a small density of nanopipes (~10/device), it was unable to model the larger leakage currents in the DUV-LED with a large density of nanopipes (~1100/device).

Further analyses of the DUV-LED IV characteristics and single nanopipe IV characteristics revealed rectifying behavior in the leakage current. Defect-sensitive etching suggested that the nanopipes do not thread entirely through the p-type GaN capping layer of the DUV-LED heterostructures. The termination of the nanopipes at or within the p-GaN layer was attributed to the enhanced lateral growth often observed in Mg-doped GaN.

Therefore, these nanopipes form p-n junctions with an inherently p-type nanopipe and the p-GaN layer, producing a non-linear current leakage effect. The three-diode circuit model was modified with the addition of a series resistor and diode in parallel with the p-n junction of the DUV-LEDs, and was then able to accurately emulate the IV characteristics of high nanopipe density DUV-LEDs. This study demonstrates the impact that nanopipes can have on the electrical characteristics and ultimately the performance of DUV-LEDs.

Sandia National Laboratories is a multi-program laboratory managed and operated by Sandia Corporation, a wholly owned subsidiary of Lockheed Martin Corporation, for the United States Department of Energy's National Nuclear Security Administration under contract DE-AC04-94AL85000.

REFERENCES

[1] P. Hart, S. Gorman, and J. Finlay-Jones, Nat. Rev. Immunol. **11,** 584 (2011).

[2] M. A. Würtele, T. Kolbe, M. Lipsz, A. Külberg, M. Weyers, M. Kneissl, and M. Jekel, Water Research **45,** 1481 (2011).

[3] Q. Li, P. K. Dasgupta, H. Temkin, M. H. Crawford, A. J. Fischer, A. A. Allerman, K. H. A. Bogart, and S. R. Lee, Appl. Spectrosc. **58,** 1360 (2004).

[4] S. Abe, S. Sato, E. Ito, M. Tsukuda, M. Tomiyama, and E. Ohno, Jpn. J. Appl. Phys. **41,** 1704 (2002).

[5] G. Roelkens, P. Dumon, W. Bogaerts, D. Van Thourhout, and R. Baets, IEEE Photonic Tech. L. **17,** 2613 (2005).

[6] H. Hirayama, S. Fujikawa, N. Noguchi, J. Norimatsu, T. Takano, K. Tsubaki, and N. Kamata, Phys. Status Solidi A **206,** 1176 (2009).

[7] S. Vilhunen, H. Särkkä, and M. Sillanpää, Environ Sci Pollut Res **16,** 439 (2009).

[8] H. Hirayama, T. Yatabe, N. Noguchi, and N. Kamata, Electronics and Communications in Japan **93,** 24 (2010).

[9] C. Pernot, M. Kim, S. Fukahori, T. Inazu, T. Fujita, Y. Nagasawa, A. Hirano, M. Ippommatsu, M. Iwaya, and S. Kamiyama, Appl. Phys. Express **3,** 061004 (2010).

[10] M. A. Khan, M. Shatalov, H. P. Maruska, H. M. Wang, and E. Kuokstis, Jpn. J. Appl. Phys. **44,** 7191 (2005).

[11] A. Touhidul Islam, N. Murakoshi, T. Fukuda, H. Hirayama, and N. Kamata, Phys. Status Solidi C **11,** 832 (2014).

[12] J. Hsu, M. Manfra, R. Molnar, B. Heying, and J. Speck, Appl. Phys. Lett. **81,** 79 (2002).

[13] C. Hartmann, J. Wollweber, A. Dittmar, K. Irmscher, A. Kwasniewski, F. Langhans, T. Neugut, and M. Bickermann, Jpn. J. Appl. Phys. **52,** 08JA06 (2013).

[14] H. Hirayama, T. Yatabe, N. Noguchi, T. Ohashi, and N. Kamata, Appl. Phys. Lett. **91,** 071901 (2007).

[15] H. Amano, A. Miyazaki, K. Iida, T. Kawashima, M. Iwaya, S. Kamiyama, I. Akasaki, R. Liu, A. Bell, and F. Ponce, Phys. Status Solidi A **201,** 2679 (2004).

[16] M. Kneissl, T. Kolbe, C. Chua, V. Kueller, N. Lobo, J. Stellmach, A. Knauer, H. Rodriguez, S. Einfeldt, Z. Yang, N. M. Johnson, and M. Weyers, Semicond. Sci. Tech. **26,** 014036 (2011).

[17] D. Cherns, Journal of Physics: Condensed Matter **12,** 10205 (2000).

[18] S. Lee, D. Oh, H. Goto, J. Ha, H. Lee, T. Hanada, M. Cho, T. Yao, S. Hong, H. Lee, S. Cho, J. Choi, J. Choi, J. Jang, J. Shin, and J. Lee, Appl. Phys. Lett. **89,** 132117 (2006).

[19] K. Shiojima and T. Suemitsu, Journal of Vacuum Science & Technology B: Microelectronics and Nanometer Structures **21,** 698 (2003).

[20] X. A. Cao, J. A. Teetsov, F. Shahedipour-Sandvik, and S. D. Arthur, J. Cryst. Growth **264,** 172 (2004).

[21] S. Hong, T. Yao, B. Kim, S. Yoon, and T. Kim, Appl. Phys. Lett. **77,** 82 (2000).

[22] S. Hong, B. Kim, H. Park, Y. Park, S. Yoon, and T. Kim, J. Cryst. Growth **191,** 275 (1998).

[23] X. Cao, J. Teetsov, M. D'Evelyn, D. Merfeld, and C. Yan, Appl. Phys. Lett. **85,** 7 (2004).

[24] B. Kim, D. Moon, K. Joo, S. Oh, Y. K. Lee, Y. Park, Y. Nanishi, and E. Yoon, Appl. Phys. Lett. **104,** 102101 (2014).

[25] M. Hawkridge and D. Cherns, Appl. Phys. Lett. **87,** 221903 (2005).

[26] D. Cherns and M. Hawkridge, Philos. Mag. **86,** 4747 (2006).

[27] D. Cherns and M. Hawkridge, J. Mater. Sci. **41,** 2685 (2006).

[28] M. Engelhardt, http://www.linear.com/designtools/software/, 2014.

[29] S. R. Lee, A. M. West, A. A. Allerman, K. E. Waldrip, D. M. Follstaedt, P. P. Provencio, D. D. Koleske, and C. R. Abernathy, Appl. Phys. Lett. **86,** 241904 (2005).

[30] J. J. Wierer, I. Montaño, M. H. Crawford, and A. A. Allerman, J. Appl. Phys. **115,** 174501 (2014).
[31] J. J. Wierer, A. A. Allerman, I. Montaño, and M. W. Moseley, Appl. Phys. Lett. **105,** 061106 (2014).
[32] M. Moseley, A. Allerman, M. Crawford, J. J. Wierer, M. Smith, and L. Biedermann, J. Appl. Phys. **116,** 053104 (2014).
[33] T. Markvart and L. Castaner, *Solar cells: materials, manufacture and operation* (Elsevier, 2004).
[34] E. Miller, D. Schaadt, E. Yu, C. Poblenz, C. Elsass, and J. Speck, J. Appl. Phys. **91,** 9821 (2002).
[35] Z. Liliental-Weber, J. Electron Microsc. **49,** (2000).
[36] Q. Sun, A. Selloni, T. H. Myers, and W. A. Doolittle, Phys. Rev. B **73,** 155337 (2006).
[37] B. Beaumont, S. Haffouz, and P. Gibart, Appl. Phys. Lett. **72,** 921 (1998).
[38] A. Yankovich, A. Kvit, X. Li, F. Zhang, V. Avrutin, H. Liu, N. Izyumskaya, Ü. Özgür, H. Morkoc, and P. Voyles, J. Appl. Phys. **111,** 023517 (2012).